Genome-Protective Topoisomerase 2a-Dependent G_2 Arrest Requires p53 in hTERT-Positive Cancer Cells

Nicola Lockwood[1], Silvia Martini[1], Ainara Lopez-Pardo[1], Katharina Deiss[1], Hendrika A. Segeren[1], Robert K. Semple[2], Ian Collins[3], Dimitra Repana[4,5], Mathias Cobbaut[1], Tanya Soliman[6], Francesca Ciccarelli[4,5], and Peter J. Parker[1,5]

ABSTRACT

Topoisomerase 2a (Topo2a)-dependent G_2 arrest engenders faithful segregation of sister chromatids, yet in certain tumor cell lines where this arrest is dysfunctional, a PKCε-dependent failsafe pathway can be triggered. Here we elaborate on recent advances in understanding the underlying mechanisms associated with this G_2 arrest by determining that p53–p21 signaling is essential for efficient arrest in cell lines, in patient-derived cells, and in colorectal cancer organoids. Regulation of this p53 axis required the SMC5/6 complex, which is distinct from the p53 pathways observed in the DNA damage response. Topo2a inhibition specifically during S phase did not trigger G_2 arrest despite affecting completion of DNA replication. Moreover, in cancer cells reliant upon the alternative lengthening of telomeres (ALT) mechanism, a distinct form of Topo2a-dependent, p53-independent G_2 arrest was found to be mediated by BLM and Chk1. Importantly, the previously described PKCε-dependent mitotic failsafe was engaged in hTERT-positive cells when Topo2a-dependent G_2 arrest was dysfunctional and where p53 was absent, but not in cells dependent on the ALT mechanism. In PKCε knockout mice, p53 deletion elicited tumors were less aggressive than in PKCε-replete animals and exhibited a distinct pattern of chromosomal rearrangements. This evidence suggests the potential of exploiting synthetic lethality in arrest-defective hTERT-positive tumors through PKCε-directed therapeutic intervention.

Significance: The identification of a requirement for p53 in stringent Topo2a-dependent G_2 arrest and engagement of PKCε failsafe pathways in arrest-defective hTERT-positive cells provides a therapeutic opportunity to induce selective synthetic lethality.

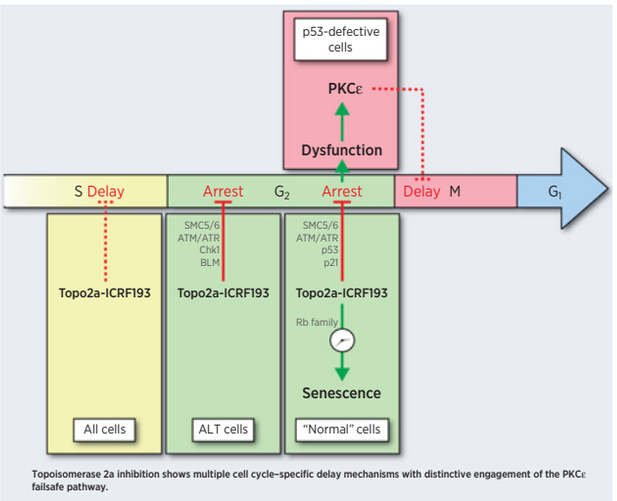

Topoisomerase 2a inhibition shows multiple cell cycle–specific delay mechanisms with distinctive engagement of the PKCε failsafe pathway.

Introduction

The Topo2a-dependent G_2 arrest is a poorly understood control mechanism that is defective in numerous tumor-derived cell lines (1, 2). This arrest mechanism is triggered by Topo2 inhibitors such as ICRF193 and, if compromised, triggers emergent dependence on PKCε failsafe pathways, wherein loss or inhibition of PKCε drives division failure (3).

The limited insight into this control mechanism is in part attributed to the multiple context-dependent responses that ICRF193 has been shown to elicit. Through its characteristic strand passage reaction, Topo2a is required for several biological processes, including the resolution of topological problems associated with DNA replication (4–7) and in the maintenance of telomeres in cells dependent upon the alternative lengthening of telomeres (ALT) pathway (8–12). Furthermore, ICRF193 has historically been used to drive genotoxicity and a G_2 DNA damage response (DDR; refs. 13–15), although observations in normal, diploid human cell lines show no overt DNA damage associated with its use (1, 2).

The distinctive cellular behaviors consequent to Topo2a ICRF193 inhibition indicate that the elicited "stress" responses vary, reflecting either a common Topo2a-associated control pathway interpreted distinctly under different conditions or the triggering of specific cellular responses indicative of distinctive molecular contexts. A recent

[1]Protein Phosphorylation Laboratory, The Francis Crick Institute, 1 Midland Road, London, UK. [2]Centre for Cardiovascular Science, University of Edinburgh, Edinburgh, UK. [3]Division of Cancer Therapeutics, The Institute of Cancer Research, London, UK. [4]Cancer Systems Biology Laboratory, The Francis Crick Institute, London, UK. [5]School of Cancer and Pharmaceutical Sciences King's College London, New Hunt's House, Guy's Campus, London, UK. [6]Barts Cancer Institute, Queen Mary University London, Charterhouse Square, London, UK.

Note: Supplementary data for this article are available at Cancer Research Online (http://cancerres.aacrjournals.org/).

N. Lockwood and S. Martini contributed equally to this work.

Current address for H.A. Segeren: Department of Biomolecular Health Sciences, Faculty of Veterinary Medicine, Utrecht University, Utrecht, the Netherlands.

Corresponding Author: Peter J. Parker, Protein Phosphorylation Laboratory, The Francis Crick Institute, 1 Midland Road, London NW1 1AT, UK. E-mail: Peter.Parker@crick.ac.uk

Cancer Res 2022;82:1762–73

doi: 10.1158/0008-5472.CAN-21-1785

screen for Topo2a-dependent G_2 arrest regulators provides a framework to assess this functionally (2). In this screen, p21 was identified as a nonredundant component in the ICRF193-induced G_2 arrest in diploid RPE1 cells, while not impacting a bleomycin-induced arrest. The p53–p21 mediated arrest has been well characterized in the DDR pathway, and prior studies focused on DNA damage involved the use of ICRF193 to identify p53 as a player in this response (13). It is unclear whether these findings are reflective of a DDR or a parallel pathway with some shared components, and if the latter, whether the mechanism is conserved in all Topo2a engagement contexts. Here we provide compelling evidence that there are context-dependent, distinctive parallel pathways that differentially engage the PKCε-protective pathway when compromised.

Materials and Methods

Reagents, biological and computational resources

For a full list of reagents and computational resources, see Supplementary Table S1. For a full list of cell lines, see Supplementary Table S2. All cell lines have been authenticated by short tandem repeat (STR) profiling and *Mycoplasma* screened by a PCR-based approach by Cell Services at The Francis Crick Institute.

Cell synchronization

For studies of S phase a single thymidine block was performed. Cells were cultured for 16 hours in growth medium supplemented with 2.5 mmol/L thymidine and subsequently washed and released into growth medium containing 1xEmbryoMax nucleosides. For all other synchrony experiments, a double thymidine block was performed as described previously (2).

Drug treatments

Unless otherwise indicated, the following drug concentrations were used in all experiments: ICRF193 3 μmol/L, bleomycin 10 μmol/L, nocodazole 1 μmol/L, Chk1 inhibitor CCT244747 1 μmol/L, Chk2 inhibitor CCT2415331 1 μmol/L, ATM inhibitor 10 μmol/L, ATR inhibitor 10 μmol/L, camptothecin 1 μmol/L, hydroxyurea 4 mmol/L, 0.5 μmol/L BLU577, and 1 μmol/L BIM-1.

EdU Click-iT proliferation assay

Cells were incubated with 10 μmol/L EdU for 30 minutes, then fixed and permeabilized with PHEM buffer (60 mmol/L PIPES pH6.8, 25 mmol/L HEPES pH7.4, 10 mmol/L EGTA pH8, 4 mmol/L $MgSO_4$, 4% paraformaldehyde, and 0.1% Triton X-100) for 20 minutes. Cells were then incubated with Click-iT reaction mix containing 1 mmol/L $CuSO_4$, 1 mmol/L Azide Alexa-Fluor 488 or 546, and 100 mmol/L ascorbic acid in PBS.

Flow cytometry

Cells were fixed in ice-cold 70% ethanol for at least 30 minutes and then permeabilized with 0.1% Triton X-100. Cell staining and subsequent analysis were performed using anti-MPM2-Cy5 and propidium iodide as described previously (2).

Immunoblotting and immunoprecipitation

Whole-cell lysates were obtained by sonication of cells in ice-cold RIPA buffer (2) or 9 M Urea (9 M Urea, 150 mmol/L 2-mercaptoethanol, 50 mmol/L TRIS-Cl pH7.5) supplemented with cOmplete EDTA-free Protease Inhibitor Cocktail, PhosSTOP, and 1 mmol/L PMSF. Lysates were run with 1× NuPAGE LDS-sample buffer.

Insoluble extracts were obtained by lysis on ice for 10 minutes in 5× pellet volumes of 1% Triton X-100 buffer (1% Triton X-100, 150 mmol/L NaCl, 50 mmol/L Tris pH7.4 and supplemented with cOmplete EDTA-free Protease Inhibitor Cocktail). Lysates were subjected to centrifugation (13,000 × *g*, 4°C, 10 minutes), and insoluble pellets were resuspended in 2× NuPAGE LDS-sample buffer (Invitrogen).

Immunoprecipitation was performed as described in (2), with the addition of PhosSTOP in the RIPA buffer and incubating the supernatant with anti–phospho-p53 (Ser15) antibodies.

Proteins were separated by SDS-PAGE and transferred to either PVDF or nitrocellulose membranes. Membranes were blocked and incubated with primary antibody at 4°C overnight in either 5% fat-free milk dissolved in PBS + 0.1% Tween 20 (PBST) or with 2.5% BSA in PBST. Antibodies were detected using HRP-conjugated secondary anti-rabbit and anti-mouse antibodies and Luminata HRP substrate or SuperSignal West Dura Extended Duration Substrate. A representative image of at least three experiments is shown. Band densitometry was performed using FIJI software and normalized to the appropriate control, as described in figure legends.

Immunofluorescence imaging and analysis

Immunofluorescence experiments, G_2 determination, and colocalization analysis were performed as described in (2). Primary antibodies used and the addition of DAPI or phalloidin are indicated in figure legends. Proliferating cell nuclear antigen (PCNA) in synchronized cells was quantified as previously described (16).

Immunofluorescence signal intensity for p53, phospho-Ser15, or γH2AX was quantified using a custom-built script and the commercial software package MATLAB. Maximum intensity projections were made of serial z-stack images spanning the entire nucleus. Individual nuclei were identified through DAPI segmentation, background was removed via thresholding, and the fluorescence signal per nucleus was calculated. Normalization to the untreated control was used to account for biological replicates. At least 30 cells were analyzed per experiment, and the mean and SEM of at least four experiments were quantified.

Binucleate determination was performed blinded to treatments, manually counting >100 cells per condition. For the decoded data, the mean and SEM of three experiments was quantified.

Mitotic trap assay

Unless otherwise indicated, cells were treated with 3 μmol/L ICRF193 or 10 μmol/L bleomycin in combination with 1 μmol/L nocodazole for 18 hours. Data are normalized to the nocodazole-alone condition.

Organoid establishment, sequencing, and culture

Colorectal cancer organoids were established from fresh colorectal cancer tissues (Human Tissue Act License numbers 12121, REC 12-EE-0493, and 18-EE-0025). The establishment and propagation of the organoids were based on previously published protocols (17). Somatic mutations for the p53-mutant sample were determined by the South London Medicine Centre, and genomic DNA for the p53 WT organoid was sequenced by the Advanced Sequencing Facility at The Francis Crick Institute.

Colorectal organoids (see Supplementary Table S2) were seeded by resuspension in basement membrane extract (BME) with media (70:30 ratio). Plates were left for 30 minutes at 37°C and 5% CO_2 for BME to solidify before the addition of media supplemented with 10 μmol/L Rock inhibitor Y-27632. For passaging, organoids were dissociated by resuspension in TrypLE Express for 15 minutes at 37°C. Dissociation was stopped by addition of 5% FBS, organoids were further disrupted

by pipetting multiple times, and then filtered through a 70-μm cell strainer before replating.

siRNA transfection

Cells were reverse transfected with a final concentration of 20 nmol/L of the indicated siRNAs using Lullaby according to the manufacturer's guidelines. Where multiple transfections were performed, the concentration of each siRNA was 20 nmol/L, and single transfections were complemented with nontargeting control siRNA. Seventy-two hours of siRNA-mediated knockdown was used for all experiments. All siRNAs are specified in Supplementary Table S1.

Tumor-prone mouse model and analysis

Studies in animals were approved by the Animal Ethics Committee of the Francis Crick Institute and the UK Home Office. p53/PKCε mice were generated in the Biological Research Facility at The Francis Crick Institute crossing C57BL/6J Trp53^{tm1Brd} with C57BL/6J Prkce^{tm1Bsca} following ARRIVE guidelines. Mice were culled at the onset of tumor-associated symptoms, such as breathing difficulties.

DNA was isolated from frozen or from formaldehyde fixed tumor tissues using the AllPrep DNA/RNA/Protein Mini Kit (Qiagen) and AllPrep DNA/RNA FFP Kit (Qiagen), respectively. 1× Low-pass genome sequencing was performed by the Advance Sequencing Facility of The Francis Crick Institute, and copy number estimation was performed using the QDNASeq package (18).

For histopathology, samples were processed and analyzed in the Experimental Histopathology facility of The Francis Crick Institute. Tumor samples were fixed in 10% NBF for 24 hours and changed into 70% ethanol. Samples were embedded in FFPE, tissues were sectioned and stained with H&E, caspase-3 (rabbit anti-caspase-3; R&D Systems, AF835) and Ki-67 (rabbit ant-KI67; Abcam, ab15580). Stained tissues were examined, and mitotic index (number of mitoses per ten ×40 fields), KI-67 index, and caspase-positive cells were quantified (percentage positive per ×40 field, counted in regions with highest positive density).

Statistical analyses

A one-way analysis of variance (ANOVA) or two-way ANOVA was used for experiments with one or two independent variables, respectively, both with multiple comparison adjustment. Student *t* tests were used to compare two sets of independent data. Where data have been normalized, a one-sample *t* test has been used to compare to the normalized control set at 1. The statistical test for each experiment is indicated in the figure legends. Prism software was used for all calculations, and the level of statistical significance is represented as follows: not significant (ns) = $P > 0.05$; *, $P \le 0.05$; **, $P \le 0.01$; ***, $P \le 0.001$; ****, $P \le 0.0001$. All statistical tests were two-sided. Sample size for each experiment is displayed in the legend.

Data availability

The genomics data generated in this study are accessible at BioProject ID PRJNA807509. Custom Built MATLAB codes for immunofluorescence quantification can be found at https://codeocean.com/capsule/5586424/tree/v1.

Results

p21 and p53 are nonredundant regulators of the Topo2a-dependent G_2 arrest

A previous RNAi screen showed knockdown of p21 abrogated the ICRF193-induced Topo2a-dependent G_2 arrest and not the

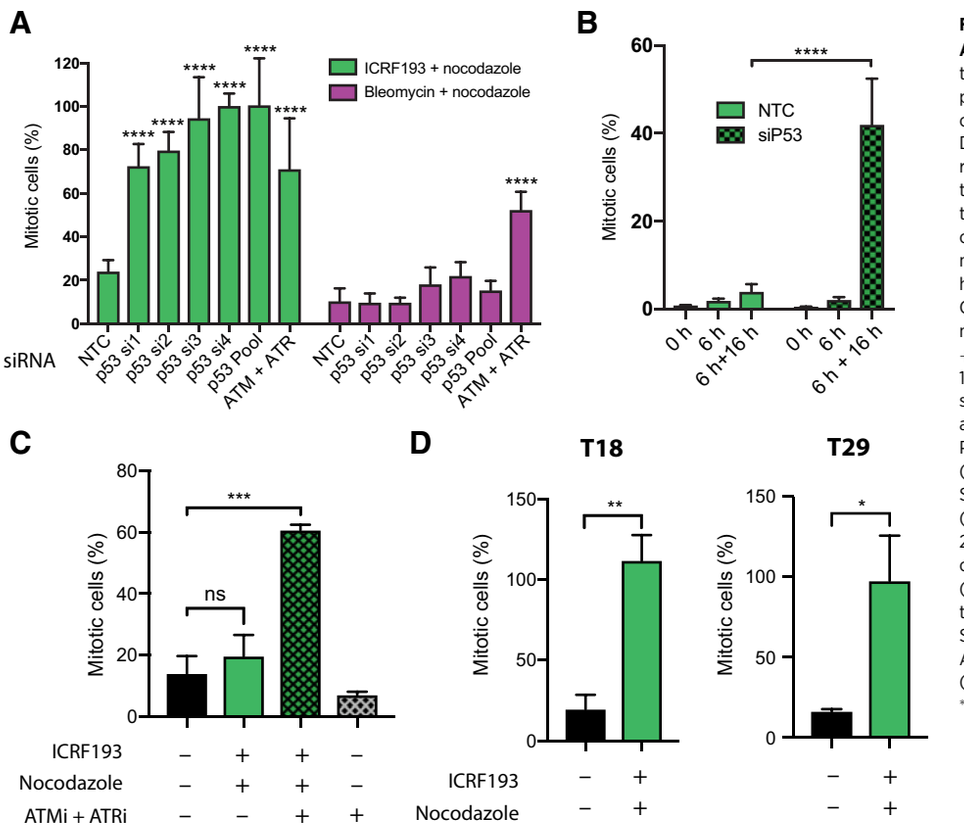

Figure 1.

A, Mitotic trap assay of RPE1 cells transfected with individual siRNAs, pools, or a nontargeting control (NTC) or positive control (siATM + siATR). Data represented as mean ± SD of a representative experiment with 6 technical replicates. **B,** RPE1 cells were transfected with nontargeting control or p53 OnTargetPlus siRNA, synchronized with a double thymidine block (0 h), released for 6 hours (6 h) to reach G_2, and then treated with ICRF193 + nocodazole for a further 16 hours (6 h + 16 h). Data were normalized to 6 h + 16 h nocodazole-alone condition and show mean ± SEM. **A** and **B,** $n = 3$; analysis by two-way ANOVA. **C** and **D,** Patient-derived colorectal organoids (described in Supplementary Table S2) that were either p53 wild-type (**C**) or mutant (**D**) were treated for 24 hours with ICRF193, nocodazole, or ATM inhibitor with ATR inhibitor (ATMi + ATRi). Data were normalized to nocodazole alone and show mean ± SEM, $n = 3$ (in **C**, ATMi + ATRi $n = 2$). Analysis (**C**) a one-way ANOVA and (**D**) a *t* test. *, $P \le 0.05$; **, $P \le 0.01$; ***, $P \le 0.001$; ****, $P \le 0.0001$.

bleomycin-induced DDR in RPE1 cells (2), a finding substantiated independently using a mitotic trap assay (Supplementary Fig. S1A and S1B). Interestingly, the p21 inducer p53 was not identified in the RNAi screen (2). This was a false negative, as deconvolution of the p53 siRNA pool used in the screen and new siRNA oligonucleotides showed that p53 loss abrogated the ICRF193-induced G_2 arrest but not the DDR (**Fig. 1A**; Supplementary Fig. S1C–S1E). Importantly, the p53 requirement for efficient ICRF193-induced arrest manifests in G_2 (**Fig. 1B**; Supplementary Fig. S1F).

To assess the penetrance of dependence, we performed a mitotic trap assay on an array of cancer cell lines with different p53 states (19). We found that cells were unable to efficiently arrest in response to ICRF193 when there was no wild-type p53 present; furthermore, the G_2 arrest was lost completely when cells were p53 null. Importantly, the bleomycin-induced G_2 arrest was completely functional in all cell lines tested (**Table 1**; Supplementary Fig. S1G).

To validate these observations in a tumor model, we performed a mitotic trap assay in patient-derived colorectal organoids that were either p53 WT or p53 mutant (Supplementary Table S2). The p53 WT organoid arrested in G_2 in response to ICRF193 in an ATM- and ATR-dependent manner (**Fig. 1C**). In agreement with the cell line data, the p53-mutant organoids did not efficiently arrest in response to ICRF193 treatment (**Fig. 1D**).

Distinct regulation of p53 in the Topo2a-dependent G_2 arrest by the SMC5/6 complex

Despite being dispensable for implementing the DDR G_2 arrest, both p53 and p21 are upregulated in response to damage (20, 21). Previous reports demonstrate that Chk1/Chk2 alone can initiate a G_2 arrest when cells are subjected to DNA damage and may work redundantly with p53 (15); hence, we anticipated differential engagement of Chk1 and Chk2. We confirmed that loss or inhibition (22, 23) of Chk1 and Chk2, either independently or in combination, was not sufficient to bypass either the ICRF193- or bleomycin-induced G_2 arrest in normal p53-replete RPE1 cells (**Fig. 2A**; Supplementary Fig. S2A–S2C). However, we observe a loss in the G_2 arrest triggered by DNA damage when either p53 or p21 are knocked down in combination with Chk1 (**Fig. 2A**; Supplementary Fig. S2D). This redundancy is a G_2 behavior, as only the combined treatment (p53 knockdown and Chk1 inhibition) bypassed the bleomycin-induced arrest in synchronized cells (**Fig. 2B**; Supplementary Fig. S2E). In agreement with this, we detected phosphorylation of Chk1 and Chk2 at residues responsible for their activation (Chk1-Ser345 and Chk2-Thr68; refs. 24, 25) when cells were treated with bleomycin, but not with ICRF193 (**Fig. 2C**).

In response to DNA damage, p53 expression is regulated by Ser15 and Ser20 phosphorylation by ATM/ATR and Chk2, respectively (21, 26–29). These phosphorylation events alongside increased expression of p53 and p21 were observed with bleomycin-induced DNA damage, with γH2AX signal verifying DNA damage (**Fig. 2D**; Supplementary Fig. S2F–S2H). ICRF193 treatment resulted in an increase of p53 and p21 expression and detectable Ser15 phosphorylation that is absent in untreated cultures (**Fig. 2D**; Supplementary Fig. S2F–S2H). However, no Ser20 phosphorylation was observed (**Fig 2D**; Supplementary Fig. S2H). Importantly, there was no DNA damage in these normal diploid cell lines with ICRF193 treatment, consistent with the conclusion that this is a distinct pathway (**Fig 2D**; Supplementary Fig. S2H).

The nonrequirement of Chk1/Chk2 may reflect an unusual single arm of the G_2 DDR pathway working through p53 regulation in response to ICRF193-inhibited Topo2a. To address this, we used fibroblast cells derived from a patient with severely reduced levels of NSE2 (a subunit of the SMC5/6 complex) resulting from a rare germline mutation (30), that are compromised in their Topo2a-dependent G_2 arrest (2). Using control NSE2 WT fibroblast cells, we observe an increase in p53 expression and Ser15 phosphorylation with

Table 1. p53 status of cells and their response to ICRF193.

Cell line	TP53 status	Details	Topo2a-dependent G_2 arrest?	DNA damage G_2 arrest?
hTERT-RPE1	WT	N/A	Complete arrest	Complete arrest
HFF	WT	N/A	Complete arrest	Complete arrest
BJ	WT	N/A	Complete arrest	Complete arrest
hTERT-BJ	WT	N/A	Complete arrest	Complete arrest
A549	WT	N/A	Complete arrest	Complete arrest
U2OS	WT	N/A	Complete arrest	Complete arrest
NCI H460	WT	N/A	Complete arrest	Complete arrest
HCC-4006	WT	N/A	Partial arrest	Complete arrest
NCI-H647	Mutant	c.782+1G>T (splice donor mutation)	Partial arrest	Complete arrest
NCI-H2170	Mutant	R158G	Partial arrest	Complete arrest
NCI-H1975	Mutant	R273H	Partial arrest	Complete arrest
NCI H522	Mutant	P191fs	Partial arrest	Complete arrest
NCI-H2228	Mutant	Q331*	Partial arrest	Complete arrest
DLD-1	Mutant	S241F	No arrest	Complete arrest
ES2	Mutant	S241F	No arrest	Complete arrest
NCI-H727	Mutant	InF Ins9c	No arrest	Complete arrest
NCI-H520	Mutant	W146*	No arrest	Complete arrest
NCI-H1703	Mutant	E285K	No arrest	Complete arrest
NCI-H1792	Mutant	c.672+1G>A (splice donor mutation)	No arrest	Complete arrest
NCI-H1299	Null	Partial deletion	No arrest	Complete arrest
HeLa	"Null"	HPV18 E6 degrades protein	No arrest	Complete arrest

Note: The published p53 status of the cells screened for their ability to arrest in response to ICRF193 is indicated. The nature of the induced arrest is color coded as shown. The arrest of cells in response to bleomycin (DNA-damage G_2 arrest) is also indicated (see **Fig. 1** and text for further details).
Abbreviation: N/A, not applicable.

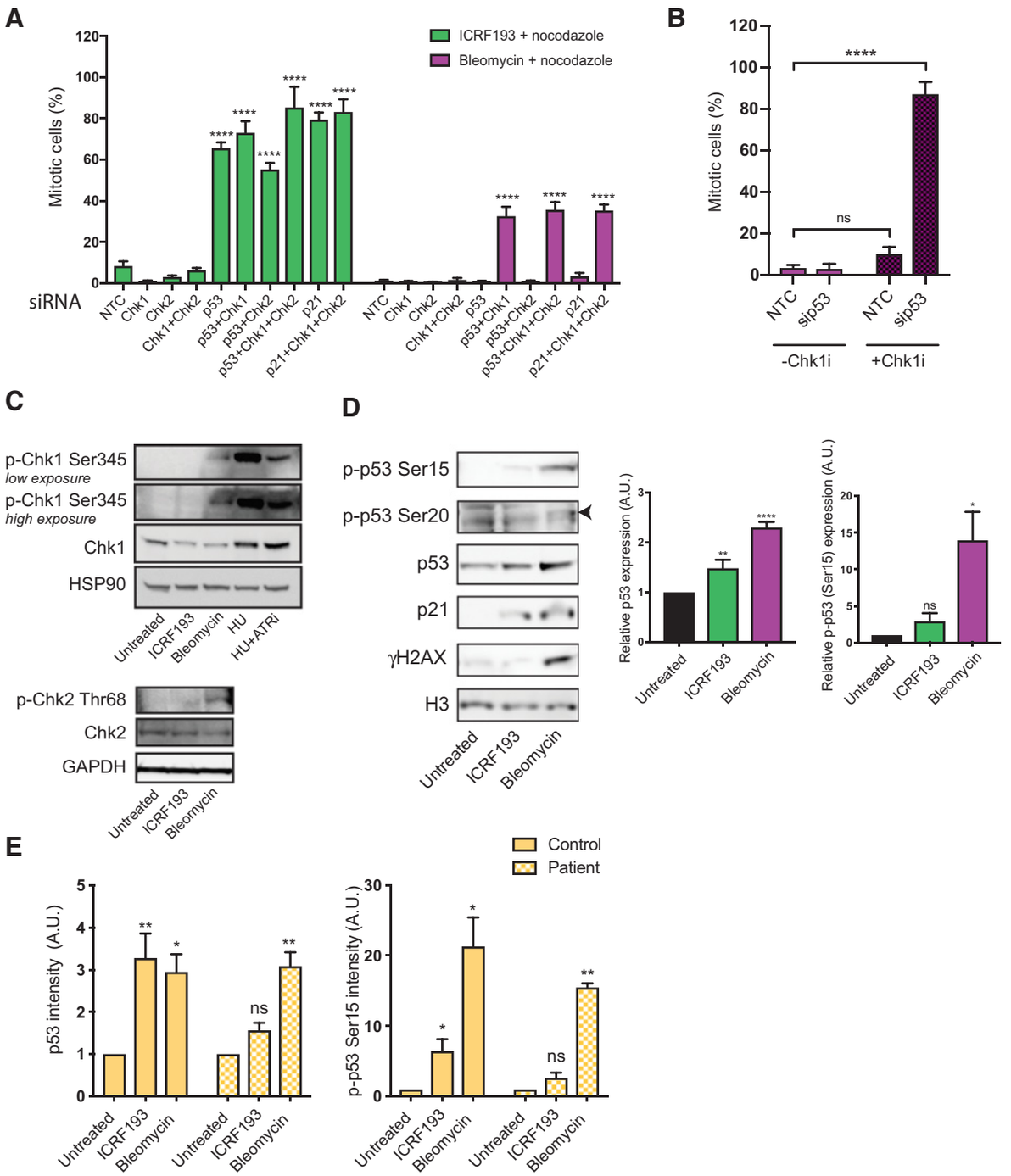

Figure 2.

A, Mitotic trap assay of RPE1 cells transfected with the indicated siRNAs. Data are represented as mean ± SD of a representative experiment with 6 technical replicates. **B,** RPE1 cells were transfected with nontargeting control (NTC) or p53 OnTargetPlus siRNA (sip53), synchronized with a double thymidine block, released for 6 hours (G_2 phase), and treated with bleomycin and nocodazole and with Chk1 inhibitor CCT244747 (Chk1i) where indicated for a further 16 hours. Data were normalized to 16 hours of nocodazole alone and show mean ± SEM. **A** and **B,** $n = 3$; analysis by two-way ANOVA. **C** and **D,** Western blots of RPE1 nuclear extracts after 18-hour treatment with ICRF193, bleomycin, 2.5 mmol/L hydroxyurea (HU), or ATR inhibitor (ATRi). Representative experiments of $n = 3$ are shown. Arrowhead, band of interest. Graphs denote the mean ± SD; $n = 3$. p53 levels were normalized to GAPDH expression and phospho-p53 at Ser15 (p-p53 Ser15) expression was normalized to p53 expression. Normalization to the untreated control accounted for biological replicates. Statistical analysis was performed using a one-sample *t* test. **E,** Quantification of immunofluorescent expression per nucleus of p53 or phospho-p53 at Ser15 (p-p53 Ser15) of control or patient fibroblasts when treated with ICRF193 or bleomycin. Patient fibroblasts were NSE2 mutant (p.Ser116Leufs*18/p.Ala234Glufs*4). Data are represented as mean ± SEM, $n = 4$, where at least 30 cells were quantified/condition. Data were normalized to the untreated control and analyzed by a one-sample *t* test.

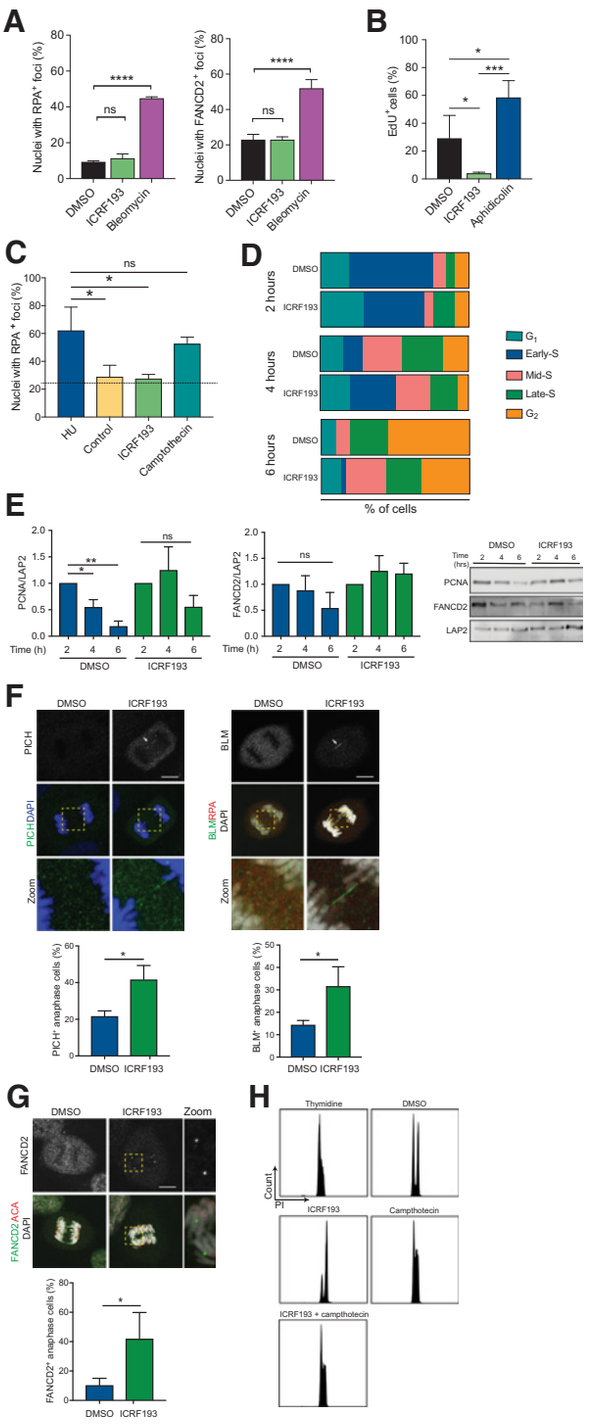

Figure 3.

A, Graphs represent the percentage of RPE1 nuclei with RPA2/32 (RPA; left) or FANCD2 (right) foci. Cells were ICRF193- or bleomycin-treated for 18 hours. At least 50 cells/condition/experiment quantified. Analysis by two-way ANOVA. **B,** Quantification of EdU-positive RPE1 cells DMSO, ICRF193, or 0.5 μmol/L aphidicolin treated for 16 hours. At least 100 cells/condition/experiment were quantified. Analysis performed by one-way ANOVA. **C,** RPE1 synchronized in G_1–S, released with hydroxyurea (HU) for 45 minutes and incubated with hydroxyurea, ICRF193, or camptothecin. Graphs show the quantification of RPA-positive foci/nuclei for each treatment. Dotted lines indicate the percentage of nuclei of asynchronous cells containing RPA foci; analysis was by one-way ANOVA. **D,** PCNA nuclear distribution (cell percentage) from G_1 to G_2. RPE1 cells synchronized in G_1–S, released with DMSO or ICRF193 for 2, 4, or 6 hours. At least 100 cells/condition quantified. **E,** Western blot of insoluble extracts from cells synchronized in G_1–S and released with DMSO or ICRF193 for 2, 4, or 6 hours. Graphs showing PCNA (right) and FANCD2 (left) normalized to LAP2 expression. Analysis performed by *t* test. **F,** Representative images of RPE1 cells synchronized in G_1–S and ICRF193-treated for 4 hours. Left, PICH (green); right, RPA (red) and BLM (green). DNA detected with DAPI. Arrows, ultrafine bridges; zoom, PICH or BLM bridges. Scale bar, 10 μm. Quantification of PICH-positive (left) and BLM-positive (right) ultrafine bridges in DMSO- or ICRF193-treated cells. Twenty anaphase cells/condition/experiment were scored; analysis by *t* test. **G,** FANCD2 (green) and centromeres (ACA; red) staining in RPE1 cells synchronized in G_1–S, 4 hours ICRF193-treated, and monitored into mitosis. Zoom, FANCD2 sister foci. Scale bar, 10 μm. Twenty anaphase cells/condition/experiment were scored. Statistical analysis by *t* test. **H,** DNA content of RPE1 cells synchronized in G_1–S and released with ICRF193 or camptothecin for 6 hours. **A–H,** Data are represented as mean ± SEM; $n = 3$. *, $P \le 0.05$; **, $P \le 0.01$; ***, $P \le 0.001$; ****, $P \le 0.0001$; ns, not significant.

ICRF193 treatment, but this is not observed in the NSE2-mutant patient-derived cells (**Fig. 2E**; Supplementary Fig. S2I and S2J). Importantly, the bleomycin-induced DDR is functional within these NSE2-mutant patient cells (**Fig. 2E**; Supplementary Fig. S2I–S2L). To provide further evidence on the distinctiveness of upstream triggers, we used siRNA targeting p53, Topo2a, and SMC6 in combination with Chk1 and Chk2 and performed mitotic trap assays in RPE1 cells. SMC6 and Topo2a do not act in concert with Chk1 and Chk2 in DDR (Supplementary Fig. S2M).

The evidence indicates that the pathway engaged to implement the ICRF193-induced G_2 arrest is a nonredundant Topo2a, SMC5/6 complex, ATM/ATR, p53, p21 regulatory cascade. Moreover, the requirements of this pathway are either not essential (Topo2a, SMC5/6 complex) or act redundantly (p53, p21) with the DDR requirement for Chk1 in G_2.

Topo2a inhibition delays S-phase progression generating unresolved replication intermediates that persist in mitosis

It is possible that the Topo2a-dependent G_2 arrest arises from a G1-like DDR trigger prompted during S phase, where ICRF193 affects replication fork progression causing S-phase delay (6). Hence, we evaluated ICRF193-induced S-phase effects on the G_2 arrest. Upon ICRF193 treatment, there was no evidence of single-stranded DNA (ssDNA) or stalled replication forks in asynchronous RPE1 cells, RPA2/RPA32 (RPA), and FANCD2 staining, respectively, contrary to the effect of bleomycin (**Fig. 3A**; Supplementary Fig. S3A). Additionally, the low levels of EdU detected in ICRF193-treated cells reveal the lack of ongoing replication when Topo2a activity is compromised, unlike following replication stress induced by aphidicolin (**Fig. 3B**; Supplementary Fig. S3B).

To exclude replication as the trigger of the Topo2a-dependent G_2 arrest, we sought to determine whether recovery from replication stress is a Topo2a-dependent process. We synchronized RPE1 cells in G_1–S and treated with hydroxyurea (HU) to induce replicative stress. After HU release, cells were either fixed as a control, or allowed to recover from the induced stress for 2 hours in DMSO, ICRF193, or the Topo1 inhibitor camptothecin. RPA quantification revealed that Topo1, and not Topo2a, is involved in the replication stress recovery pathway in normal diploid cells (**Fig. 3C**). Similarly, FANCD2 staining confirmed this finding, although 2-hour release from HU was not sufficient to fully recover from the replication stress induced (Supplementary Fig. S3C).

To further investigate the potential involvement of Topo2a in DNA replication in normal diploid cells, we synchronized RPE1 cells in G_1–S and tracked S-phase progression under ICRF193 treatment. Monitoring the PCNA nuclear pattern established by the replication timing program (Supplementary Fig. S3D; ref. 16), we observed a delay in S-phase progression in ICRF193-treated cells after 4 hours, which became more evident at 6 hours (**Fig. 3D**). We confirmed this at the protein level, observing significantly higher expression of PCNA and FANCD2 in nuclear extracts obtained at 4 and 6 hours after thymidine release (**Fig. 3E**).

Replication fork progression can be problematic in some specific DNA regions such as common fragile sites (CFS), potentially leading to underreplicated DNA that engenders ultrafine bridges (UFB) connecting sister chromatids in anaphase and telophase (31). When this occurs, the mitotic DNA synthesis pathway (MiDAS) is required to resolve incomplete replication during mitosis. We monitored anaphase cells derived from a synchronized RPE1 population incubated with ICRF193 only during DNA replication and observed a significantly higher number of cells undergoing anaphase with UFBs compared with control (**Fig. 3F**), indicating the presence of underreplicated CFSs (32). Lack of RPA staining on the anaphase bridges excluded the presence of extensive regions of ssDNA (**Fig. 3F**). The presence of underreplicated DNA in mitosis was confirmed by the characteristic accumulation of FANCD2 in symmetrical foci on the chromosome arms (**Fig. 3G**) and anti-centromere antibody (ACA) staining revealed that the PICH-positive bridges caused by ICRF193 treatment were not associated with centromeres (Supplementary Fig. S3E).

p53 binding protein 1 (53BP1) is known to accumulate in foci on replication stress or incomplete replication. As previously demonstrated (16, 33), 53BP1 nuclear foci decrease through S-phase progression in normal diploid cells (Supplementary Fig. S3F). Consistent with the delay in DNA replication progression, we found that 53BP1 accumulation in nuclear foci persists through S phase upon Topo2a inhibition and colocalizes with γH2AX (Supplementary Fig. S3F), suggesting that 53BP1 is required to shield DNA lesions induced by ICRF193 during S phase. In addition, as in asynchronous cells, RPA immunostaining revealed the absence of single-strand breaks (Supplementary Fig. S3G). It is noted that the sustained ICRF193 inhibition of Topo2a into G_2 leads to loss of the S-phase γH2AX staining (**Fig. 2D**; Supplementary Fig. S2G and S2H), indicative of resolution of these lesions during the arrest.

Collectively, these data indicate that Topo2a inhibition through S phase affects completion of DNA replication generating regions of underreplicated DNA that can be tolerated, do not trigger the S-phase checkpoint, nor the Topo2a-dependent G_2 arrest and can persist into mitosis. However, the bulk of DNA synthesis is completed before the ICRF193-mediated G_2 arrest, as demonstrated by the DNA incorporation profile (**Fig. 3H**). By contrast, Topo1 inhibition by camptothecin triggers an S-phase arrest that is not influenced by Topo2 inhibition, indicating the dominant role of Topo1 in S-phase DNA topological stress resolution (**Fig. 3H**).

ALT-dependent cells have an alternative Chk1-mediated Topo2a-dependent G_2 arrest

We observe an efficient G_2 arrest in ICRF193-treated U2OS cells (**Fig. 4A**; ref. 2), despite previous publications reporting they have compromised p53 signaling, lack a functional G_1 DDR, and their G_2 DDR is reliant upon Chk1 (15, 34). U2OS cells are p53 WT, but they have an active, truncated form of the phosphatase Wip1 (34), which we confirmed is present in our U2OS cell line (Supplementary Fig. S4A).

The ICRF193-mediated G_2 arrest in U2OS cells is dependent upon known regulators of the Topo2a-dependent G_2 arrest; ATM/ATR and all components of the SMC5/6 complex (**Fig. 4B**). Knockdown of p53 does not abrogate the ICRF193- or bleomycin-induced G_2 arrest in U2OS cells, consistent with the weakened p53 signaling previously described (**Fig. 4C**). However, we observed a dependence upon Chk1 with both ICRF193 and bleomycin treatment in U2OS cells, starkly contrasting with normal, diploid cell lines (**Fig. 4C**; Supplementary Fig. S4B). Furthermore, upon ICRF193 treatment, U2OS cells display Chk1 phosphorylation at Ser345 (**Fig. 4D**), in contrast to RPE1 cells (**Fig. 2C**), in addition to an increase in p53 and p21 (Supplementary Fig. S4C).

Unlike other p53-defective cell lines studied here, U2OS cells are reliant upon ALT activity for telomere maintenance and immortality. Topo2a activity has been implicated previously in the ALT mechanism (8, 10, 12); furthermore, ALT is reliant upon impaired p53 signaling and is reported to be dependent upon the SMC5/6 complex (35, 36). To assess whether the ALT pathway correlates with this idiosyncratic arrest dependency, we investigated additional ALT cell lines, SAOS2 and GM847. Both initiated a partial arrest after ICRF193 treatment (Supplementary Fig. S4D); however, this arrest, as in U2OS cells, was completely abrogated with the addition of a Chk1 inhibitor (Supplementary Fig. S4E). We hypothesize that Topo2a inhibition affects telomere maintenance in ALT cells initiating an independent, distinct G_2 arrest that, while dependent upon the ATM/ATR + SMC5/6 complex, relies upon Chk1 activity.

A recent study has described a BLM-dependent G_2–M arrest in ALT cells, which occurred alongside an increase in telomere recombination intermediate dissolution and a subsequent increase in ALT phenotypes, including ALT-associated PML bodies (APB; ref. 37). Topo2a has previously been found in a complex with BLM and TRF2 in ALT cells and can enhance BLM activity *in vitro* (8, 11). We confirmed that the ICRF193-mediated G_2 arrest was dependent on BLM in U2OS cells and GM847 cells, but importantly this dependence was not observed in the normal, diploid cell line RPE1 (**Fig. 4E**; Supplementary Fig. S4F and S4G). In addition, ICRF193-treated U2OS cells reproduced the increase in APBs previously observed with hyper-ALT activity (**Fig 4F**; Supplementary Fig. S4H). These were also dependent on BLM presence and were not purely indicative of G_2-arrested cells (Supplementary Fig. S4I and S4J). Chk1 activity is not required for the formation or maintenance of the hyper-ALT APBs, indicating a downstream role in the ICRF-induced arrest (**Fig 4F**; Supplementary Fig. S4H). Interestingly, we found the ICRF193-induced G_2 arrest in ALT-dependent cells also led to G_2 cellular senescence, but not as rapidly as observed in normal, diploid cells (Supplementary Fig. S4K and S4L).

PKCε is engaged when the Topo2a-dependent G_2 arrest is compromised by loss of the p53–p21 in hTERT-positive cancer cells

We have previously identified three PKCε-regulated events that provide genome protection in cell lines with a compromised Topo2a-dependent G_2 arrest (3). As p53 and p21 are essential for the Topo2a-dependent G_2 arrest in normal, diploid cells, we tested whether experimental loss of p53 resulted in a dependence on PKCε for faithful chromosome segregation in RPE1 cells. The combination of ICRF193 and either of two structurally distinct inhibitors that can target PKCε, BLU577, and BIM-1 led to an increased number of binucleated cells only when either p53 or p21 were subjected to siRNA-mediated knockdown (**Fig 5A**).

To determine whether a bypass in the ALT-associated ICRF193-induced arrest in U2OS cells also engendered reliance upon

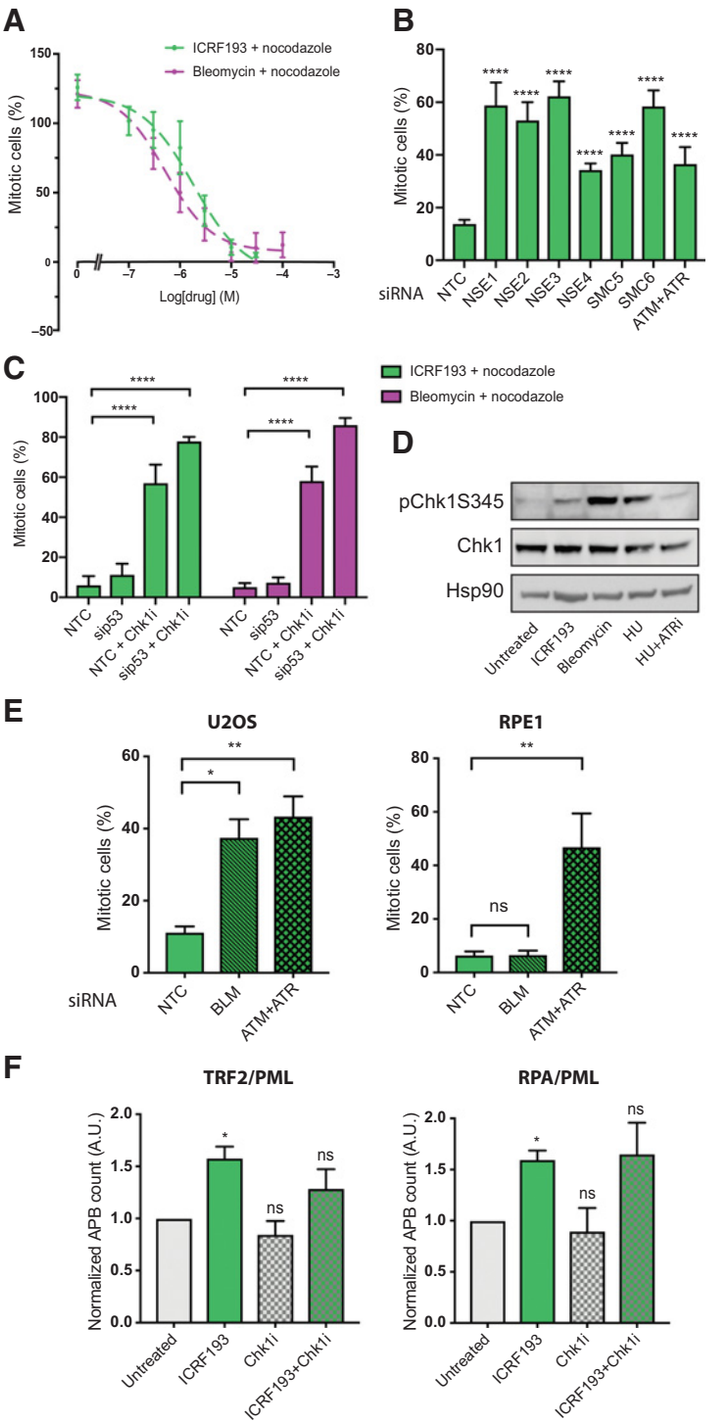

Figure 4.

A, U2OS cells treated with ICRF193 or bleomycin + nocodazole for 24 hours. Mitotic cells mean ± SD are from a representative experiment with 8 technical replicates; $n = 3$. **B,** Mitotic trap assay of U2OS cells transfected with the indicated siRNAs. Data are represented as mean ± SD of a representative experiment with 6 technical replicates, $n = 3$; analysis by one-way ANOVA. **C,** U2OS cells were transfected with control (NTC) or p53 siRNA (sip53), synchronized in G_1–S, released for 10 hours and treated for 16 hours with ICRF193 or bleomycin + nocodazole and Chk1 inhibitor CCT244747 (Chk1i) where indicated. Mitotic index mean ± SEM normalized to 16 hours of nocodazole, $n = 3$; analysis by two-way ANOVA. **D,** Western blots of U2OS cell extracts after 18 hours of ICRF193, bleomycin, ATR inhibitor (ATRi), or 2.5 mmol/L hydroxyurea (HU) treatment. A representative experiment of 3 is shown. **E,** Mitotic trap assay of U2OS and RPE1 cells transfected with control (NTC), siBLM, or siATM + siATR and treated with ICRF193 + nocodazole for 18 hours. Mitotic cells counts mean ± SEM, $n \geq 3$; analysis one-way ANOVA. **F,** MATLAB-aided quantification of APBs (colocalization of TRF2 or RPA) in U2OS cells after 18 hours of treatment with ICRF193 and Chk1 inhibitor CCT244747 (Chk1i). Data normalized to untreated controls are mean ± SEM; $n = 3$; analysis t test. *, $P \leq 0.05$; **, $P \leq 0.01$; ****, $P \leq 0.0001$; ns, not significant.

PKCε action, we scored the occurrence of failed division when Chk1 and PKCε were inhibited in combination. The loss of Chk1 activity resulted in an increase in binucleates, but this was not exacerbated by PKCε inhibition (**Fig. 5B**). Consistent with this, we observed an increase in DAPI-positive bridges indicative of segregation errors with ICRF193 and Chk1 inhibitor treatment, which was also not exacerbated by PKCε inhibition (Supplementary Fig. S5A and S5B). Loss of the Topo2a-dependent arrest in ALT cells does not engage a PKCε-dependent failsafe pathway.

p53–PKCε display a genetic interdependence *in vivo*

To test the potential for PKCε and p53 to express a functional relationship *in vivo*, and in the absence of PKCε-selective drugs with suitable pharmacokinetic properties, we sought to test the impact of

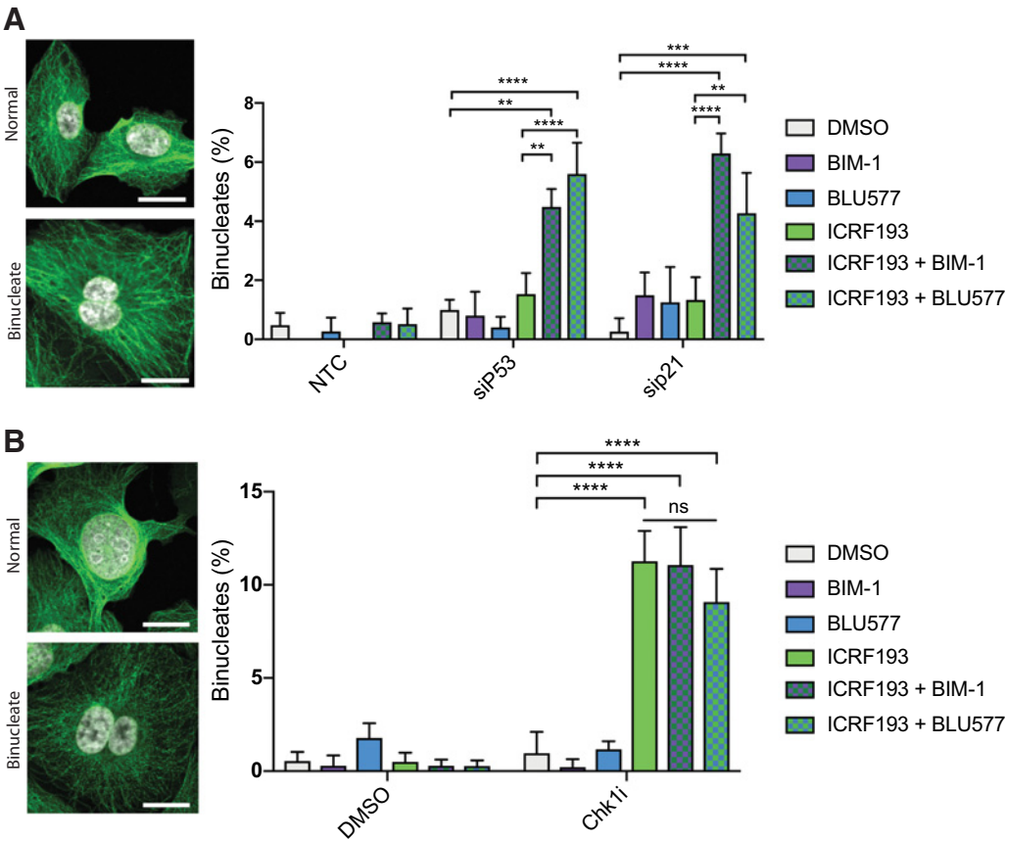

Figure 5.

A and **B,** Representative confocal images show normal or binucleate cells with tubulin (green) and DAPI (white) staining. Scale bar, 20 μm. Data are represented as mean ± SEM; ≥ 100 cells/experiment, $n = 3$; analysis by two-way ANOVA. **A,** RPE1 cells were transfected with nontargeting control (NTC), siP53 OnTargetPlus, or siP21 and were treated with DMSO, ICRF193, BLU577, or BIM-1 for 16 hours. **B,** U2OS cells were synchronized with a single thymidine block, released for 10 hours, and then treated when in G_2 with DMSO, Chk1 inhibitor CCT244747 (Chk1i), ICRF193, BLU577, or BIM-1 for 16 hours. **, $P \leq 0.01$; ****, $P \leq 0.0001$; ns, not significant.

PKCε loss on tumors driven by p53 loss. Germline deletion of p53 in mice results in spontaneous tumorigenesis, mostly thymic $CD4^+CD8^+$ T-cell lymphomas (38). We observed that lack of PKCε in the p53-null tumor-prone model affected the age of tumor formation and survival, as *Trp53*$^{-/-}$*Prkce*$^{-/-}$ mice developed lymphoblastic lymphoma earlier than the *Trp53*$^{-/-}$*Prkce*$^{+/+}$mice (17.6 weeks vs. 19.6 weeks, on average). However, PKCε germline deletion resulted in a less invasive phenotype, as *Trp53*$^{-/-}$*Prkce*$^{-/-}$ mice were found with enlarged thymi only. By contrast, *Trp53*$^{-/-}$*Prkce*$^{+/+}$ mice developed thymic lymphomas involving other organs (**Fig. 6A**). IHC revealed elevated cell proliferation in the thymic samples from both genotypes, alongside caspase-3 activation (Supplementary Fig. S6A).

We assessed CNVs in these lymphomas, and in accordance with recent studies (39, 40), the karyotypic landscape from the *Trp53*$^{-/-}$*Prkce*$^{+/+}$ tumors displayed aneuploidy for multiple chromosomes, including chromosome 4 and 5 gain and chromosome 13 loss (**Fig. 6B**), aneusomies identified also in human lymphoblastic lymphomas (41). Although the *Trp53*$^{-/-}$*Prkce*$^{-/-}$ karyotype showed less whole-chromosome changes compared with the PKCε wild-type, the whole amplification of some specific chromosomes (such as chromosome 4, 5, 11, 14, and 15) and the reduction of chromosomes losses (Supplementary Fig. S6B and S6C) were consistently found among the samples analyzed. In addition, we observed a higher number of intrachromosomal gains, especially on chromosome 12 and 4, and decreased intrachromosomal deletion events in *Trp53*$^{-/-}$*Prkce*$^{-/-}$, compared with the *Prkce*$^{+/+}$ (**Fig. 6C** and **D**).

Discussion

The study has determined that among the complex responses to Topo2 inhibition by the noncovalent catalytic inhibitor ICRF193, the cellular response is not governed by a singular signal relay, but by a context-dependent pattern of responses differentiated from the DDR. For the S phase, inhibition results in a delay to S-phase transition and an element of underreplication insufficient to trigger a G_2 arrest, but if not resolved by the MiDAS pathway and carried through to anaphase results in PICH- and BLM-positive UFBs. In ALT cells, we demonstrate that the G_2 arrest observed is dependent upon the SMC5/6 complex, ATM/ATR, BLM, and Chk1. By contrast, the characteristic arrest observed in normal cells and hTERT immortalized cells is dependent upon the SMC5/6 complex, ATM/ATR, p53, and p21. Notably, the distinct relays also differentially engage the downstream failsafe pathway under PKCε control. Thus, for cells by-passing the p53-dependent G_2 arrest, there is an exacerbation of consequent division failure triggered by PKCε inhibition, which is not present in ALT cells. Finally, we demonstrate that there is a genetic

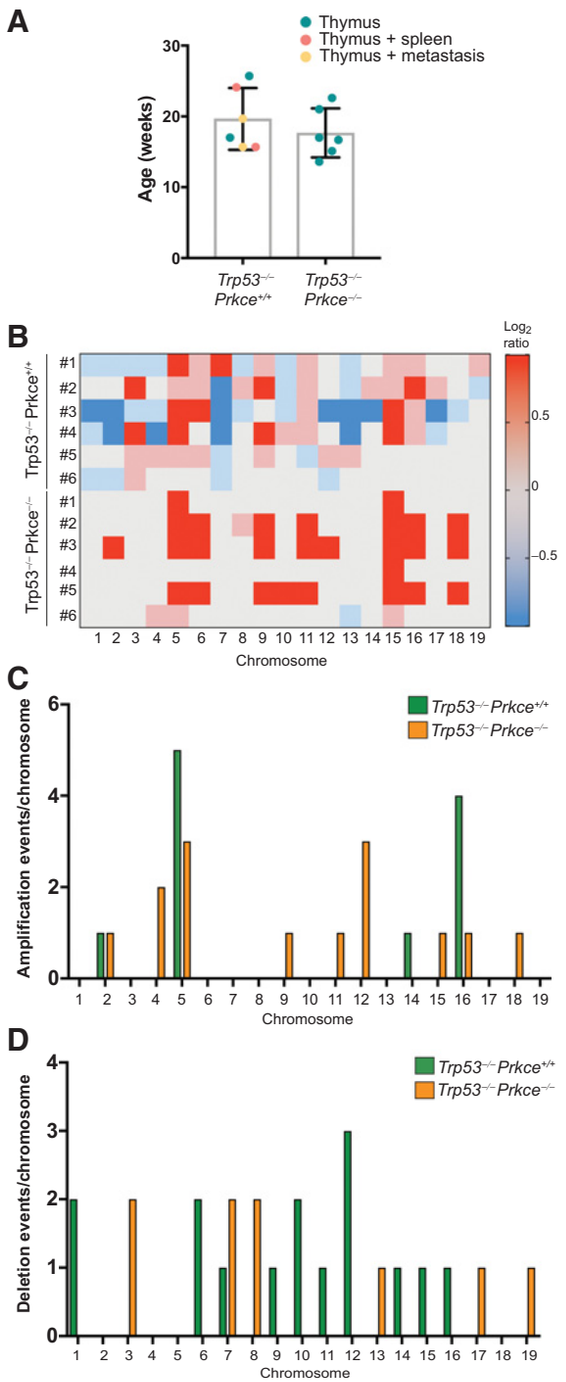

Figure 6.

A, Graph showing the age of death (weeks) of *Trp53*$^{-/-}$*Prkce*$^{+/+}$ and *Trp53*$^{-/-}$*Prkce*$^{-/-}$ mice. Mice showing enlarged thymus only (blue), thymus and spleen (pink), and thymus and metastasis (yellow). **B,** Heat map showing DNA copy number changes in tumors from *Trp53*$^{-/-}$*Prkce*$^{+/+}$ and *Trp53*$^{-/-}$*Prkce*$^{-/-}$. Values are presented for each chromosome (*x*-axis) from each mouse (*y*-axis) as a $\log_2$ ratio of amplification (red) or deletion (blue). **C** and **D,** Graphs indicating single amplification or deletion events (*y*-axis) within each chromosome (*x*-axis) in the *Trp53*$^{-/-}$*Prkce*$^{+/+}$ (green) and *Trp53*$^{-/-}$*Prkce*$^{-/-}$ (orange) mice.

interdependence of p53 and PKCε *in vivo* in respect of the selection of specific chromosome aberrations associated with lymphomas, consistent with the functional relationship observed in the *ex vivo* models.

The requirement of p53 for a proficient Topo2a-dependent G_2 arrest is in agreement with a previous observation in normal human fibroblasts (NHF; ref. 13); however, we show that this behavior is not a result of ICRF193-induced DNA damage or genotoxicity as previously concluded. However, our findings contrast with a study concluding that p53 is dispensable for an ICRF193-induced G_2 arrest after 2 hours of treatment in NHFs (42), indicating that there may be a p53-independent acute phase delay that precedes a p53-dependent G_2 arrest. Interestingly, data within this previous study support this notion, where p53 loss in the NHF7 line results in an increased proportion of cells evading the drug-induced G_2 delay after just 2 hours of ICRF193 treatment, which may reflect the acute window. We note that there are exceptions to this p53 arrest requirement. Conversely, cells that are p53 WT may lack a functional Topo2a-dependent G_2 arrest response and be reliant upon PKCε-failsafe mechanisms due to deficiencies elsewhere in the signaling cascade.

The involvement of p53 rationalizes why the cellular context in which the ICRF193-induced G_2 arrest is studied is important. A substantial proportion of the literature on this arrest response has been conducted in p53-mutant or compromised cell lines, such as HeLa (14, 43), where the dominant effect of ICRF193 is at the metaphase-to-anaphase transition (44). This could contribute to the differences in reported genes involved in the G_2 arrest and the observed engagement of the DDR (in the absence of a robust arrest, ICRF193 will trigger aberrant divisions and their consequences). This issue is exemplified in the use of HeLa cells to assess the levels of γH2AX as a readout for damage after ICRF193 treatment (15, 45). The involvement of p53 can also account for the differential segregation errors observed upon treatment with ICRF193, with previous studies contrastingly demonstrating ICRF159, a structural relative of ICRF193, induced mostly centromeric UFBs when using cells immortalized with SV40 large T antigen that inhibits p53 function (46, 47).

The identification of a distinct Topo2a-dependent G_2 arrest in ALT cells clarifies the previous contradictory results demonstrating Chk1 involvement (15). The SMC5/6 complex has previously been shown to be essential for APB formation, ALT cell proliferation, and maintenance (36), and previous studies have also shown that Topo2a inhibition or knockdown causes an increase in telomere-damage–induced foci (TIF), an additional ALT cell marker (9, 12). Therefore, we hypothesize that compromised Topo2a activity drives an increase in ALT-related properties with respect to APBs and a subsequent Chk1-mediated G_2 arrest, elaborating upon the previously observed G_2 arrest in response to an imbalance of dissolution at ALT telomeres. This Topo2a-dependent G_2 arrest in ALT cells questions our previous conclusions, based upon the use of inducible U2OS cell lines to assess Topo2a mutants (2). It was concluded that SUMOylation of the novel site K1520 was not essential for a Topo2a-dependent G_2 arrest but was involved in resolution. We cannot sustain this conclusion, but the observation indicates that Topo2a SUMOylation at this site may also help facilitate resolution of ALT telomere intermediates. Using both RPE1 and primary patient-derived NSE2-mutant cells, we have previously shown that the E3 SUMO ligase activity is critical for both the G_2 arrest and Topo2a-K1520 SUMOylation in response to ICRF193 (2). Therefore, it is likely that this SUMOylation site is required for a stringent Topo2a-dependent G_2 arrest in normal, diploid cells, but this needs to be confirmed.

Although the agents exploited here to block selective PKCε activity are inadequate for assessing the impact of inhibition in the context of p53-defective tumors *in vivo*, we have provided evidence that there is an interdependence of p53 and PKCε in tumor development. Although this might be a tumor microenvironment consequence of PKCε loss, the finding that less aggressive tumors form when PKCε is absent and that there are consistent tumor-autonomous changes in chromosome alterations are consistent with tumor cell loss of the underlying PKCε-dependent genome-protective pathway. This conclusion is bolstered by the observation that similar altered chromosomal changes were recently described in tumors isolated from mice where loss of p53 is combined with inactivation of the spindle assembly checkpoint protein Mad2 (40).

Although it remains to be determined what is being monitored in the cells to trigger the non-ALT G_2 arrest pathway, the characterization of this important Topo2a-dependent G_2 arrest offers a promising therapeutic opportunity. Given that p53 is the most frequently mutated gene in human cancer, and where it is not mutated its activity is typically compromised (48), many cancers will engage PKCε to support chromosome segregation. Therefore, targeting PKCε could prove beneficial therapeutically, exploiting the synthetic lethal behaviors in arrest-defective failsafe-reliant tumors. Such approaches are promising, as evident in the success of PARP inhibitors in BRCA-mutant tumors (49). Furthermore, knowing that PKCε knockout mice are viable adds the expectation that PKCε intervention would afford a good therapeutic index.

Authors' Disclosures

I. Collins reports other support from The Institute of Cancer Research, grants and personal fees from Cancer Research UK, grants from Cancer Research UK Pioneeer Fund, grants and other support from Sareum Ltd., and personal fees and other support from Sierra Oncology during the conduct of the study; grants and other support from The Institute of Cancer Research and Monte Rosa Therapeutics Inc., grants and personal fees from Cancer Research UK, grants from Merck KGaA and Medical Research Council, personal fees from Epidarex LLP, Dunad Therapeutics, Cardiff University, and nonfinancial support from Atomwise outside the submitted work; in addition, I. Collins has a patent for WO2009004329 issued and licensed to Sierra Oncology, a patent for WO2009044162 issued and licensed to Sierra Oncology, a patent for WO2009103966 pending and licensed to Sierra Oncology, a patent for WO2008075007 issued and licensed to Sierra Oncology, a patent for WO2013068755 pending and licensed to Sierra Oncology, a patent for WO2013171470 issued and licensed to Sierra Oncology, a patent for WO2010007389 pending and licensed to Cancer Research Technology Ltd., and a patent for WO2009053694 issued and licensed to Cancer Research Technology Ltd. No disclosures were reported by the other authors.

Authors' Contributions

N. Lockwood: Conceptualization, formal analysis, supervision, investigation, methodology, writing–original draft, writing–review and editing. **S. Martini:** Conceptualization, formal analysis, investigation, methodology, writing–original draft, writing–review and editing. **A. Lopez-Pardo:** Formal analysis, investigation, writing–review and editing. **K. Deiss:** Resources, formal analysis, investigation, writing–review and editing. **H.A. Segeren:** Resources, formal analysis, investigation, writing–review and editing. **R.K. Semple:** Resources, formal analysis, investigation, writing–review and editing. **I. Collins:** Resources, investigation, writing–review and editing. **D. Repana:** Resources, investigation, writing–review and editing. **M. Cobbaut:** Resources, investigation, writing–review and editing. **T.N. Soliman:** Conceptualization, resources, supervision, investigation, writing–review and editing. **F. Ciccarelli:** Conceptualization, resources, formal analysis, supervision, investigation, methodology, writing–original draft, writing–review and editing. **P.J. Parker:** Conceptualization, resources, formal analysis, supervision, investigation, methodology, writing–original draft, writing–review and editing.

Acknowledgments

This work was supported by The Francis Crick Institute, which receives its core funding from Cancer Research UK (FC001130), the UK Medical Research Council (FC001130), and the Wellcome Trust (FC001130). R.K. Semple is funded by the Wellcome Trust (grant 210752/Z/18/Z). D. Repana was supported by a Fellowship from the Health Education England Genomics Education Programme. For the purpose of Open Access, the author has applied a CC BY public copyright license to any Author Accepted Manuscript version arising from this submission. The authors would like to thank The Francis Crick Institute STPs for support with this research, in particular the High-Throughput Screening Laboratory, Light Microscopy, Flow Cytometry, Experimental Histopathology, Biological Research Facility and Cell Services. They also thank Karen Vousden and Simon Boulton for their insightful discussion and gifting reagents and acknowledge Mariia Yuneva and Kanaga Sabapathy for kindly gifting cell lines.

The costs of publication of this article were defrayed in part by the payment of page charges. This article must therefore be hereby marked *advertisement* in accordance with 18 U.S.C. Section 1734 solely to indicate this fact.

Received June 3, 2021; revised February 1, 2022; accepted February 25, 2022; published first March 1, 2022.

References

1. Downes CS, Clarke DJ, Mullinger AM, Giménez-Abián JF, Creighton AM, Johnson RT. A topoisomerase II-dependent G_2 cycle checkpoint in mammalian cells. Nature 1994;372:467–70.
2. Deiss K, Lockwood N, Howell M, Segeren HA, Saunders RE, Chakravarty P, et al. A genome-wide RNAi screen identifies the SMC5/6 complex as a non-redundant regulator of a Topo2a-dependent G_2 arrest. Nucleic Acids Res 2019;47:2906–21.
3. Parker PJ, Lockwood N, Davis K, Kelly JR, Soliman TN, Pardo AL, et al. A cancer-associated, genome protective programme engaging PKCε. Adv Biol Regul 2020; 78:100759.
4. Baxter J, Diffley JFX. Topoisomerase II inactivation prevents the completion of DNA replication in budding yeast. Mol Cell 2008;30:790–802.
5. Branzei D, Foiani M. Maintaining genome stability at the replication fork. Nat Rev Mol Cell Biol 2010;11:208–19.
6. Gaggioli V, Le Viet B, Germe T, Hyrien O. DNA topoisomerase IIα controls replication origin cluster licensing and firing time in Xenopus egg extracts. Nucleic Acids Res 2013;41:7313–31.
7. Heintzman DR, Campos VL, Byl JAW, Osheroff N, Dewar JM. Topoisomerase II is crucial for fork convergence during vertebrate replication termination. Cell Rep 2019;29:422–63.
8. Bhattacharyya S, Keirsey J, Russell B, Kavecansky J, Lillard-Wetherell K, Tahmaseb K, et al. Telomerase-associated protein 1, HSP90, and topoisomerase IIα associate directly with the BLM helicase in immortalized cells using ALT and modulate its helicase activity using telomeric DNA substrates. J Biol Chem 2009; 284:14966–77.
9. Chen L, Zhu X, Zou Y, Xing J, Gilson E, Lu Y, et al. The topoisomerase II catalytic inhibitor ICRF-193 preferentially targets telomeres that are capped by TRF2. Am J Physiol Cell Physiol 2015;308:C372–7.
10. Hsieh MH, Tsai CH, Lin CC, Li TK, Hung TW, Chang TL, et al. Topoisomerase II inhibition suppresses the proliferation of telomerase-negative cancers. Cell Mol Life Sci 2015;72:1825–37.
11. Russell B, Bhattacharyya S, Keirsey J, Sandy A, Grierson P, Perchiniak E, et al. Chromosome breakage is regulated by the interaction of the BLM helicase and topoisomerase IIα. Cancer Res 2011;71:561–71.
12. Ye J, Lenain C, Bauwens S, Rizzo A, Saint-Léger A, Poulet A, et al. TRF2 and Apollo cooperate with topoisomerase 2α to protect human telomeres from replicative damage. Cell 2010;142:230–42.
13. Baus F, Gire V, Fisher D, Piette J, Dulić V. Permanent cell cycle exit in G_2 phase after DNA damage in normal human fibroblasts. EMBO J 2003;22: 3992–4002.

14. Park I, Avraham HK. Cell cycle-dependent DNA damage signaling induced by ICRF-193 involves ATM, ATR, CHK2, and BRCA1. Exp Cell Res 2006;312:1996–2008.
15. Lossaint G, Besnard E, Fisher D, Piette J, Dulić V. Chk1 is dispensable for G_2 arrest in response to sustained DNA damage when the ATM/p53/p21 pathway is functional. Oncogene 2011;30:4261–74.
16. Spies J, Lukas C, Somyajit K, Rask MB, Lukas J, Neelsen KJ. 53BP1 nuclear bodies enforce replication timing at under-replicated DNA to limit heritable DNA damage. Nat Cell Biol 2019;21:487–97.
17. van de Wetering M, Francies HE, Francis JM, Bounova G, Iorio F, Pronk A, et al. Prospective derivation of a living organoid biobank of colorectal cancer patients. Cell 2015;161:933–45.
18. Scheinin I, Sie D, Bengtsson H, van de Wiel MA, Olshen AB, van Thuijl HF, et al. DNA copy number analysis of fresh and formalin-fixed specimens by shallow whole-genome sequencing with identification and exclusion of problematic regions in the genome assembly. Genome Res 2014;24:2022–32.
19. Bouaoun L, Sonkin D, Ardin M, Hollstein M, Byrnes G, Zavadil J, et al. TP53 variations in human cancers: new lessons from the IARC TP53 database and genomics data. Hum Mutat 2016;37:865–76.
20. Gillis LD, Leidal AM, Hill R, Lee PWK. p21 Cip1/WAF1 mediates cyclin B1 degradation in response to DNA damage. Cell Cycle 2009;8:253–6.
21. Lakin ND, Jackson SP. Regulation of p53 in response to DNA damage. Oncogene 1999;18:7644–55.
22. Anderson VE, Walton MI, Eve PD, Boxall KJ, Antoni L, Caldwell JJ, et al. CCT241533 is a potent and selective inhibitor of CHK2 that potentiates the cytotoxicity of PARP inhibitors. Cancer Res 2011;71:463–72.
23. Walton MI, Eve PD, Hayes A, Valenti MR, De Haven Brandon AK, Box G, et al. CCT244747 is a novel potent and selective CHK1 inhibitor with oral efficacy alone and in combination with genotoxic anticancer drugs. Clin Cancer Res 2012;18:5650–61.
24. Liu Q, Guntuku S, Cui XS, Matsuoka S, Cortez D, Tamai K, et al. Chk1 is an essential kinase that is regulated by Atr and required for the G_2–M DNA damage checkpoint. Genes Dev 2000;14:1448–59.
25. Matsuoka S, Rotman G, Ogawa A, Shiloh Y, Tamai K, Elledge SJ. Ataxia telangiectasia-mutated phosphorylates Chk2 in vivo and in vitro. Proc Nat Acad Sci USA 2000;97:10389–94.
26. Banin S, Moyal L, Shieh SY, Taya Y, Anderson CW, Chessa L, et al. Enhanced phosphorylation of p53 by ATM in response to DNA damage. Science 1998;281:1674–7.
27. Lakin ND, Hann BC, Jackson SP. The ataxia-telangiectasia related protein ATR mediates DNA-dependent phosphorylation of p53. Oncogene 1999;18:3989–95.
28. Shieh SY, Taya Y, Prives C. DNA damage-inducible phosphorylation of p53 at N-terminal sites including a novel site, Ser20, requires tetramerization. EMBO J 1999;18:1815–23.
29. Hirao A, Kong YY, Matsuoka S, Wakeham A, Ruland J, Yoshida H, et al. DNA damage-induced activation of p53 by the checkpoint kinase Chk2. Science 2000;287:1824–7.
30. Payne F, Colnaghi R, Rocha N, Seth A, Harris J, Carpenter G, et al. Hypomorphism in human NSMCE2 linked to primordial dwarfism and insulin resistance. J Clin Invest 2014;124:4028–38.
31. Sarlós K, Biebricher A, Petermann EJG, Wuite GJL, Hickson ID. Knotty problems during mitosis: mechanistic insight into the processing of ultrafine DNA bridges in anaphase. Cold Spring Harbor Symp Quant Biol 2017;82:187–95.
32. Chan KL, Palmai-Pallag T, Ying S, Hickson ID. Replication stress induces sister-chromatid bridging at fragile site loci in mitosis. Nat Cell Biol 2009;11:753–60.
33. Tiwari A, Addis Jones O, Chan KL. 53BP1 can limit sister-chromatid rupture and rearrangements driven by a distinct ultrafine DNA bridging-breakage process. Nat Commun 2018;9:677.
34. Kleiblova P, Shaltiel IA, Benada J, Ševčík J, Pecháčková S, Pohlreich P, et al. Gain-of-function mutations of PPM1D/Wip1 impair the p53-dependent G1 checkpoint. J Cell Biol 2013;201:511–21.
35. Dilley RL, Greenberg RA. ALTernative telomere maintenance and cancer. Trends Cancer 2015;1:145–56.
36. Potts PR, Yu H. The SMC5/6 complex maintains telomere length in ALT cancer cells through SUMOylation of telomere-binding proteins. Nat Struct Mol Biol 2007;14:581–90.
37. Panier S, Maric M, Hewitt G, Mason-Osann E, Gali H, Dai A, et al. SLX4IP antagonizes promiscuous BLM activity during ALT maintenance. Mol Cell 2019;76:27–43.
38. Donehower LA, Harvey M, Vogel H, McArthur MJ, Montgomery CA Jr, Park SH, et al. Effects of genetic background on tumorigenesis in p53-deficient mice. Mol Carcinog 1995;14:16–22.
39. Foijer F, Albacker LA, Bakker B, Spierings DC, Yue Y, Xie SZ, et al. Deletion of the MAD2L1 spindle assembly checkpoint gene is tolerated in mouse models of acute T-cell lymphoma and hepatocellular carcinoma. Elife 2017;6:e20873.
40. Shoshani O, Bakker B, de Haan L, Tijhuis AE, Wang Y, Kim DH, et al. Transient genomic instability drives tumorigenesis through accelerated clonal evolution. Genes Dev 2021;35:1093–108.
41. Haider Z, Landfors M, Golovleva I, Erlanson M, Schmiegelow K, Flægstad T, et al. DNA methylation and copy number variation profiling of T-cell lymphoblastic leukemia and lymphoma. Blood Cancer J 2020;10:45.
42. Kaufmann WK, Campbell CB, Simpson DA, Deming PB, Filatov L, Galloway DA, et al. Degradation of ATM-independent decatenation checkpoint function in human cells is secondary to inactivation of p53 and correlated with chromosomal destabilization. Cell Cycle 2002;1:210–9.
43. Lou Z, Minter-Dykhouse K, Chen J. BRCA1 participates in DNA decatenation. Nat Struct Mol Biol 2005;12:589–93.
44. Brownlow N, Pike T, Zicha D, Collinson L, Parker PJ, Gisselsson D, et al. Mitotic catenation is monitored and resolved by a PKCε-regulated pathway. Nat Commun 2014;5:5685.
45. Robinson HMR, Bratlie-Thoresen S, Brown R, Gillespie DAF. Chk1 is required for G_2–M checkpoint response induced by the catalytic topoisomerase II inhibitor ICRF-193. Cell Cycle 2007;6:1265–7.
46. Baumann C, Körner R, Hofmann K, Nigg EA. PICH, a centromere-associated SNF2 family ATPase, is regulated by Plk1 and required for the spindle checkpoint. Cell 2007;128:101–14.
47. Chan KL, Hickson ID. On the origins of ultra-fine anaphase bridges. Cell Cycle 2009;8:3065–6.
48. Zhou X, Hao Q, Lu H. Mutant p53 in cancer therapy-the barrier or the path. J Mol Cell Biol 2019;11:293–305.
49. Lord CJ, Tutt ANJ, Ashworth A. Synthetic lethality and cancer therapy: lessons learned from the development of PARP inhibitors. Annu Rev Med 2015;66:455–70.